Avoidance of ghost atoms in holographic low-energy electron diffraction (LEED)

2000 J. Phys.: Condens. Matter 12 5527

(http://iopscience.iop.org/0953-8984/12/26/301)

J. Phys.: Condens. Matter **12** (2000) 5527–5540. Printed in the UK PII: S0953-8984(00)13784-1

Avoidance of ghost atoms in holographic low-energy electron diffraction (LEED)

A Seubert†, D K Saldin‡, J Bernhardt†, U Starke† and K Heinz†§

† Lehrstuhl für Festkörperphysik, Universität Erlangen–Nürnberg, Staudtstrasse 7, D-91058 Erlangen, Germany

‡ Department of Physics and Laboratory for Surface Studies, University of Wisconsin–Milwaukee, PO Box 413, Milwaukee, WI 53201, USA

E-mail: kheinz@fkp.physik.uni-erlangen.de

Received 8 May 2000

Abstract. It is pointed out that real-space images recovered from LEED I/E data by the current holographic reconstruction algorithm can contain strong artifacts which can be misinterpreted as atomic images ('ghost atoms'), thereby misguiding a subsequent structural refinement through conventional LEED. We show that such ghost atoms can be avoided by using an alternative approximation to the kernel in the reconstruction integral. This is demonstrated for both calculated and experimental intensities of the structure considered, i.e. a (2×2) phase of 6H-SiC$(000\bar{1})$. A theory is also developed for a practical implementation of a more general kernel which fully takes account of the scattering of an electron by the substrate atoms *before* its first encounter with the adatom (beam splitter).

1. Holographic interpretation of LEED intensities

The holographic interpretation of low-energy electron diffraction (LEED) intensities was originally proposed [1] to apply to diffuse LEED patterns arising from adatoms on surfaces, regarded as beam splitters for the incoming electron beam and for the Bragg reflected waves due to prior scattering of this wave from the substrate. In terms of the three-step model of diffuse LEED [2], the reference wave, R, was regarded as the total outgoing wave from the adsorbate after step 1 of the calculation. That outgoing wave consists of two parts: one (denoted by the symbol R_1) arising from the direct back-scattering of the incident wave by the adatom; and the other (R_2) that from the scattering by the same adatom of electrons previously back-scattered from the substrate. In this picture, the object waves O are spherical waves emerging from substrate atoms as a result of the subsequent scattering by the substrate of the composite wave R $(=R_1 + R_2)$ (corresponding to step 3 of the diffuse LEED picture).

If the adatoms form a lattice gas on the substrate, the resulting diffraction pattern may be regarded as simply a more intense version of the interference pattern from a single adsorbate. Representative scattering paths of the waves R_1 and O due to a single adatom are shown as solid lines in figure 1. A DLEED pattern is the result of the interference between electrons travelling along a variety of scattering paths in the vicinity of the adsorbate. Consequently, it is characteristic of the short-range order of atoms in the vicinity of the adsorbate. One aspect of holographic LEED is at variance with the traditional view of a hologram as arising from

§ Author to whom any correspondence should be addressed.

0953-8984/00/265527+14$30.00

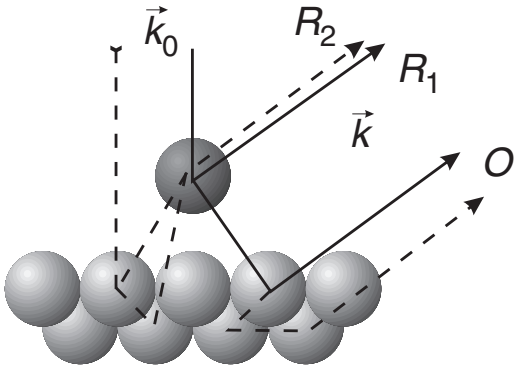

Figure 1. The beam-splitter arrangement for holographic LEED and different types of scattering process.

the interference between a *known* reference wave and an unknown object wave of arbitrary complexity. It is the presence of the R_2-term (whose scattering paths are represented by dashed lines in figure 1) that might strongly disturb that simple picture. If R_2 is considered a part of the reference wave, the latter is not completely known; if the reference wave were considered to be only the directly knowable R_1-term, R_2 would be essentially a nuisance term that disrupts the holographic picture of an interference between the reference wave, R_1, and the object wave, O.

The back-propagation picture [1] of holographic reconstruction gives a clue as to the most appropriate grouping of terms. In this picture, the reconstruction process retraces the paths of the electrons backward in time from the diffraction pattern (hologram) to the *last* scatterer [3,4], which is the same (the adatom) for both quantities, R_1 and R_2. In contrast, the object waves, O, may be regarded mainly as outgoing spherical waves from the *last* substrate atoms in the scattering paths following the electrons' last encounter with the adatom (in step 3 of the diffuse LEED picture [2]). A back-propagation image-reconstruction algorithm would lead these paths back to the positions of these last scatterers, which include all the substrate atoms, *even in the presence of multiple scattering*. This suggests that the idea of grouping R_1 and R_2 as components of a composite reference wave [1,5] is likely to be a profitable one.

In this picture, the composite reference wave R $(=R_1 + R_2)$ may be viewed as a sum of spherical waves emerging from the adatom [1], just like a photoemitted wave in photoelectron holography [6]. Consequently, it might be surmised that image-reconstruction algorithms developed for photoelectron holography might be similarly successful for holographic LEED. The most successful of these algorithms are applied to a set of photoelectron diffraction patterns of different energies. They consist of three-dimensional phased Fourier-like transforms that convert measured intensities in reciprocal space to real-space 'images' of the 3D configuration of scattering atoms in the vicinity of the photoemitter [7–9].

Direct applications of such algorithms to LEED, however, are somewhat disappointing. The characteristic perhaps most associated with holography in the popular view, a fully 3D reconstructed image, does not usually result. The strongly forward-peaked nature of the direct reference wave, R_1, tends to preferentially reconstruct images of substrate atoms in the direction of a forward-scattering cone from the adsorbate to the extent that it may drown out images of the other atoms [10–12]. A solution to this problem was subsequently proposed [5], in which a kernel is included in the image-reconstruction integral to compensate for the anisotropy of the composite reference wave $R_1 + R_2$. The estimation of the anisotropy of the R_1-term is straightforward enough: it requires only an evaluation of the adsorbate atomic scattering

factor. An exact estimation of R_2, however, is essentially impossible at the outset since the positions of the substrate atoms relative to the adatom are not known *a priori* (although one could conceive of algorithms for iteratively improving an estimate of this quantity, as discussed below). Nevertheless, quite a successful algorithm has been developed [5, 13], in which the contribution of R_2 in the kernel is approximated by a constant C, treated essentially as a parameter to be varied until a full 3D picture of atomic arrangements is visible in the reconstructed image.

For disordered adsorbates, this algorithm has been able to recover atomically well resolved real-space images from a number of adsorbate systems [13, 14]. More significantly, following earlier ideas [15, 16], the method has recently been extended [17, 18, 21] to the reconstruction of real-space images of adsorbate systems from conventional LEED intensity-versus-energy (I/E) curves of the superstructure Bragg spots that arise from an ordered overlayer of different periodicity to the substrate. This extension of the scope of holographic LEED is of considerable experimental advantage as most surface crystallography is still performed on ordered surfaces, and since Bragg spot intensities are much easier to measure in practice than weak diffuse LEED patterns. The idea exploited is the fact that the discrete intensities may be viewed as *sampling* the diffuse LEED pattern of a corresponding disordered system [19]. It has been shown that a (3×3) adatom superstructure usually gives a sufficient Bragg spot sampling density in reciprocal space to enable the recovery of the local atomic arrangements around the adatom [20]. Under favourable circumstances even a (2×2) superstructure can be sufficient [21]. The method was successfully applied to such cases of long-range order [17, 21, 22] where clear atomically resolved images could be reconstructed which have even enabled the determination of the crystallography of a previously unknown surface structure [17, 18].

Given the complicated anisotropies and energy dependences of the reference and object waves in holographic LEED, it is remarkable that the simplified kernel [5] in current use was able to identify the adatom geometry even in so complicated a surface as SiC(111) (3×3), information crucial for the solution of that structure [17]. We found subsequently that there is at least one case where a false, or 'ghost' atom can appear on an image reconstructed by such an algorithm on an axis through the reference atom perpendicular to the surface. This occurs for the structure consisting of a $(2 \times 2)_C$ silicon adatom layer on a 6H-SiC$(000\bar{1})$ surface. In section 2 we describe how the appearance of such a ghost atom had initially misguided the analysis of this structure, which was subsequently determined by a conventional LEED analysis [23]. In section 3 we revisit the arguments leading to this kernel, and derive a general expression, valid in the limit of single scattering by the substrate atoms in each of the steps 1 and 3 of a diffuse LEED calculation. We find that one set of approximations to this more general expression leads to the simplified kernel K_1 used up to the present. An alternative set of (equally arguable) approximations leads to a new practical kernel K_2. In section 4 we show that use of the new kernel K_2 enables the elimination of the ghost atoms discussed above from images reconstructed from both calculated model intensities and experimental data. Section 5 contains a discussion and conclusions.

2. Ghost atoms in reconstructed images of 6H-SiC$(000\bar{1})$-$(2 \times 2)_C$

Surfaces of silicon carbide are currently under investigation in our laboratory as this material offers a high potential for technical applications due to its unique electronic properties [24]. In the course of an investigation of the atomic structure of different phases on 6H-SiC$(000\bar{1})$ by quantitative LEED, we focused on a $(2 \times 2)_C$ phase with approximately bulk-like surface stoichiometry as monitored by Auger electron spectroscopy (AES). The index C is used to

distinguish the present phase from a different, silicon-rich $(2 \times 2)_{\mathrm{Si}}$ phase [25]. The left panel of figure 2 displays the LEED pattern for normal incidence of the primary beam at an electron energy of 95 eV. Scanning tunnelling microscopy (STM) measurements (see the right panel of figure 2) reveal a true (2×2) surface periodicity in contrast to a mixture of mutually rotated (2×1) domains also consistent with the observed LEED pattern. From both filled- and empty-state STM images we can conclude that each (2×2) unit cell contains only one protruding surface atom. This is also supported by the undistorted geometry in the vicinity of point defects and antiphase domain boundaries indicated by the circle and line inserts in figure 2, respectively.

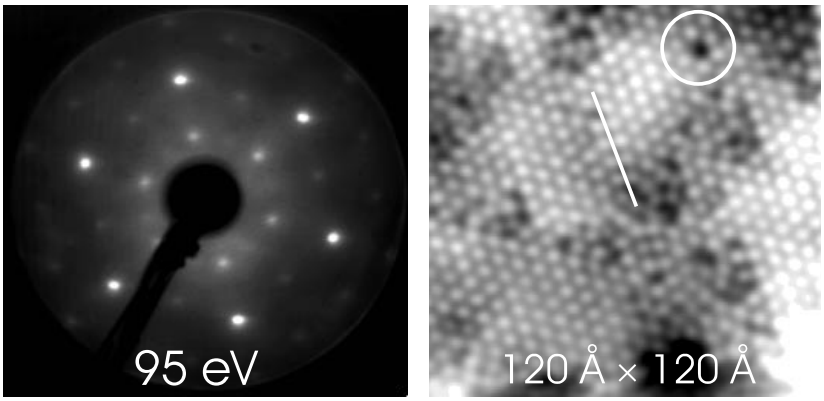

Figure 2. A LEED pattern at 95 eV (left) and a STM image for −2.75 V (right) for the $(2 \times 2)_{\mathrm{C}}$ phase of 6H-SiC(000$\bar{1}$).

The presence of a single protruding atom per unit cell is a prerequisite for the application of holographic LEED, as this atom can act as a well defined microscopic beam splitter for the incoming electron wave. So, the present case seemed to be a promising candidate for a successful application of the method. Intensity-versus-energy spectra, $I(E)$, of five half-order spots ($(\frac{1}{2}0)$, $(\frac{1}{2}\frac{1}{2})$, $(1\frac{1}{2})$, $(\frac{3}{2}0)$, $(\frac{3}{2}\frac{1}{2})$) were recorded using a computer-controlled video-LEED system [26]. They cover an energy range from at least 34 eV up to 349 eV, depending on the Bragg spot. It should be mentioned that though the sample exhibits threefold rotational symmetry (including one mirror plane), the LEED pattern is of sixfold symmetry. This is due to the presence of equally weighted domains of different surface terminations of the hexagonal 6H polytype which are rotated by 60° with respect to each other. Of course, this superposition of intensities stemming from different domains leaves the successful application of the reconstruction algorithm to some extent uncertain. In addition, the (2×2) periodicity represents—due to the low density of sampling points—a lower limit for a reliable image reconstruction.

The reconstruction was performed using the 'compensated object and reference wave reconstruction by an energy-dependent Cartesian transform' algorithm (CORRECT) [5, 13]. The real-space image $|A(\vec{r})|^2$ in the vicinity of the beam splitter located at the origin $\vec{r} = \vec{0}$ is given by

$$A(\vec{r}) = \int K(\vec{k}, \vec{r}) H(\vec{k}) \mathrm{e}^{-\mathrm{i}(kr - \vec{k}\cdot\vec{r})} \, \mathrm{d}\vec{k} \tag{1}$$

with $\vec{k}$ and $H(\vec{k})$ the wave vector and intensity of the measured electrons, respectively. The reader should note that due to the sampling of intensities at discrete Bragg spot positions $\vec{k}_{\|}$

and energies

$$E = \sqrt{\vec{k}_{\parallel}^2 + k_{\perp}^2}$$

the integral in equation (1) is a (discrete) summation rather than a (continuous) integration. One of the functions of the kernel $K(\vec{k}, \vec{r})$ in (1) is to correct for the anisotropic scattering by the beam splitter [5], without which only atoms within the forward-scattering cone of the incident wave would show up [10]. The approximate form of the kernel used up to the present has been

$$K_1(\vec{k}, \vec{r}) = \frac{r}{f_b(\vec{k}_0, \vec{r}) + C} \tag{2}$$

with $f_b(\vec{k}_0, \vec{r})$ the scattering factor of the beam-splitting atom and $\vec{k}_0$ the wave vector of the incident electrons. The quantity C was taken to represent the amplitude of the zeroth-order approximation to the scattering by the substrate before a final scattering by the adsorbate (beam splitter) [5]. In applications up to the present, this has been taken to be a free parameter, to be optimized to retrieve clear images of atoms outside the forward-scattering cone of the beam splitter [27].

The image resulting from the application of the algorithm (1) to measured LEED intensities of energy range 106–349 eV from a 6H-SiC(000$\bar{1}$)-$(2 \times 2)_C$ surface is shown in perspective in figure 3. Image intensities on a spatial grid of positions separated by 0.15 Å are represented by small spheres whose diameters and shadings are proportional to those intensities. The whole image covers a cylinder of depth 5.0 Å and radius $r_{\parallel} = 2.7$ Å both of which restrict the size of the image to being smaller than the maximum calculable from the finite sampling in reciprocal space [21]. The optimized kernel constant used in this calculation was $C = 1.4$ Å. Image noise, i.e. intensities below 30% of the maximum in the present case, was not plotted. Due to the slight silicon enrichment at the surface of the present sample, it was surmised that the beam-splitter atom in this case was Si. Yet, using the scattering factor, $f_b(\vec{k}_0, \vec{r})$, of carbon rather than that of silicon in the integral kernel did not significantly modify the result, as the angular shape of f is not very atom specific.

As expected from the LEED pattern, the real-space image exhibits sixfold rotational symmetry. Obviously, the above-mentioned coexistence of domains of different orientation does not destroy the image but leads to a superposition of images from the two domains, i.e. the hexagonal ring of atoms (labelled 1 at depth $z = -1.1$ Å in figure 3) must be interpreted as the superposition of the images from two trimers rotated by 60° with respect to each other, as indicated by the lines inserted. Consequently, we interpret the local atomic cluster from either domain as consisting of the beam-splitting atom (not shown) supported by a trimer of substrate atoms (1). This in turn is above another atom at depth $z = -1.9$ Å (labelled (2) in the figure) followed by a further on-axis atom at depth $z = -4.2$ Å (labelled (3)).

In order to refine the coordinates of the atom positions recovered by this process, and to retrieve the remaining atoms within the unit cell not detected by the holographic reconstruction, a conventional LEED intensity analysis was performed, using standard full dynamical computer programs [28, 29] as well as those employing the perturbation scheme, tensor-LEED [30, 31]. Knowing from STM that there is a single protruding atom per (2×2) surface unit cell, and not fully trusting the above image reconstruction, we tried different high-symmetry sites for that adatom, i.e., sites T_1, H_3 and T_4, displayed in figure 4(a). In the T_1 configuration, the adatom is onefold coordinated and resides on top (T) of a first-layer carbon atom. In the H_3 site, it occupies a threefold-coordinated hollow site (H). The T_4 site is characterized by the adatom being threefold coordinated to carbon atoms below *and* to the next-layer silicon atom on top (T) of which it resides, resulting effectively in a fourfold coordination. Obviously, this

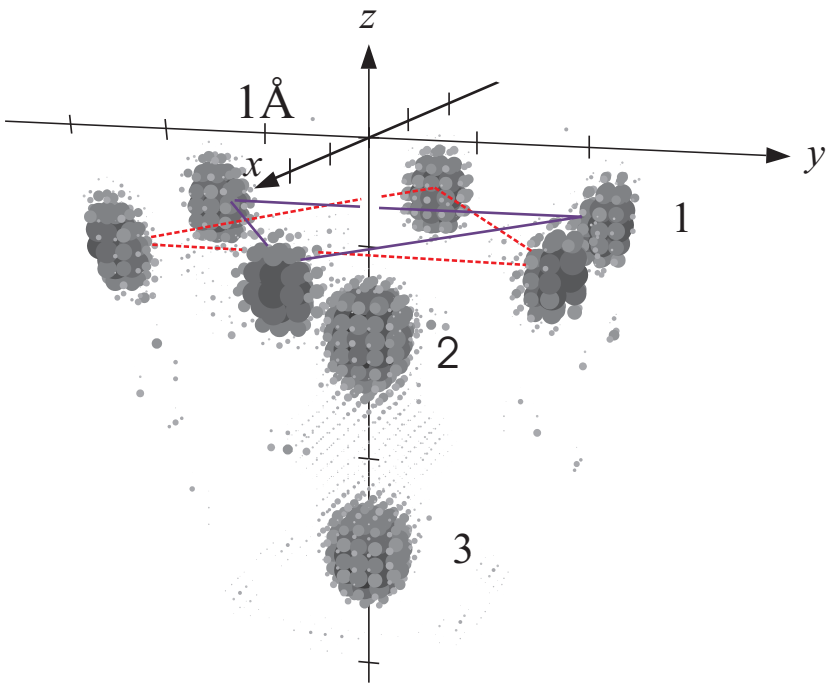

Figure 3. A real-space image obtained from holographic reconstruction of measured data for 6H-SiC(000$\bar{1}$)-(2 × 2)$_C$. See the text for more details.

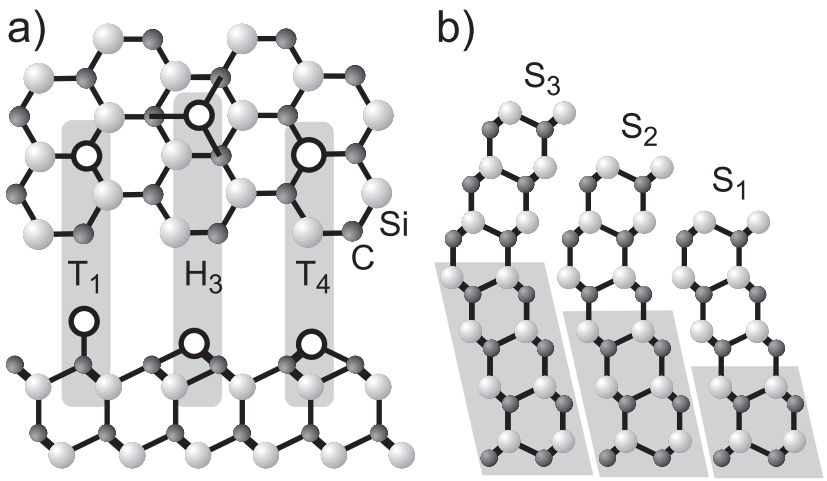

Figure 4. (a) Possible high-symmetry adsorption sites on the hexagonal surface of SiC shown in a top view and a side-view projection along the [11$\bar{2}$0] direction. Adatoms are displayed as white circles. (b) A side-view projection along [11$\bar{2}$0] of the three different surface stacking terminations S_1, S_2 and S_3 of the 6H polytype. See the text for more details.

site corresponds best to the atomic cluster reconstructed holographically above. In both the T_1 and H_3 configurations, atoms directly below the adatom are rather distant, contrary to the indication in the reconstructed image.

In addition to the different sites mentioned, the analysis had to consider different possible surface terminations of the 6H polytype. These are denoted by S_1, S_2 and S_3 where the indices refer to the number of identically oriented (i.e. linearly stacked) SiC bilayers below the surface, as indicated in figure 4(b). Each termination appears in two equally probable orientations, mutually rotated by 60°, as indicated by the shaded areas. All three stacking sequences, and their respective domain weights, as well as the different sites of the adatoms and their chemical identity (silicon or carbon) were tested in the course of the LEED analysis. Surprisingly, in view of the indication of a T_4-type atomic cluster from the holographic analysis above, and the fact that the T_4 silicon-adatom configuration has been found for e.g. the $(\sqrt{3} \times \sqrt{3})$ phase of 4H-SiC(0001) both experimentally [32] and by density functional theory (DFT) calculations [33, 34], the T_4 configuration failed to produce a satisfactory fit to the experimental LEED intensity-versus-energy (I/E) spectra. Instead, the best fit with a Pendry R-factor [35] of $R_P = 0.20$ was found for a silicon adatom in an H_3 geometry on a dominantly S_1-terminated surface, as displayed in figure 5 in top (upper panel) and side views (lower panel). More details of the structure determination and the precise structural parameters are given elsewhere [23].

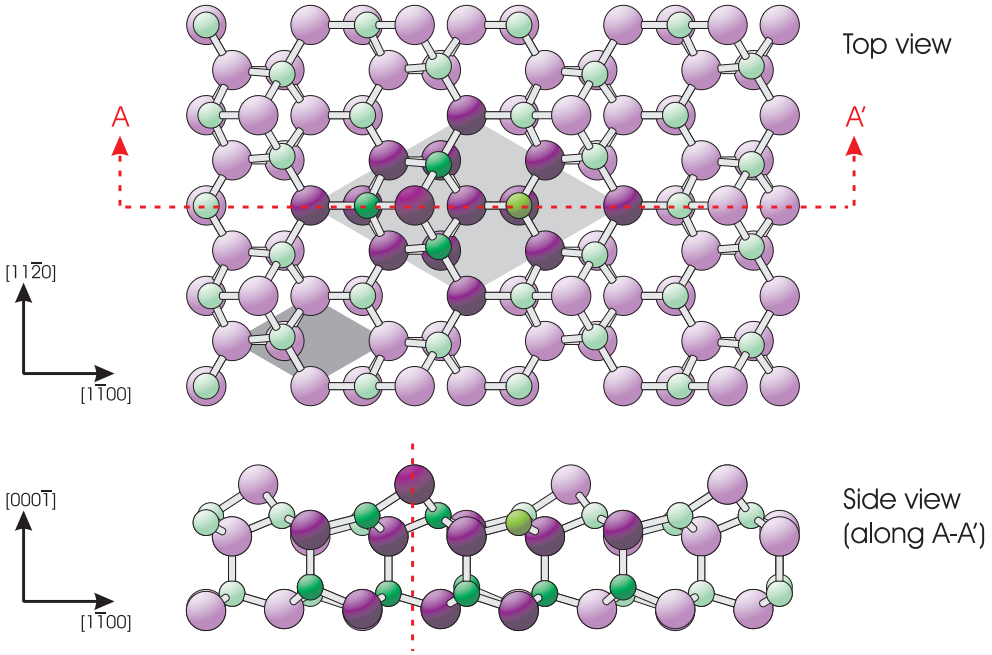

Figure 5. The best-fit structure model of the $(2 \times 2)_C$ phase on 6H-SiC(000$\bar{1}$) in a top view (upper panel) and side view (lower panel). Both panels depict the dominant S_1 surface termination.
(This figure is in colour only in the electronic version, see `www.iop.org`)

Obviously, the adatom geometry obtained by conventional LEED is in clear conflict with the holographically reconstructed image. The latter suggests the presence of an atom about $z = -2.0$ Å below the beam-splitting adatom. As this atom is missing in the structure reliably determined by conventional LEED, it must be an artifact of the image reconstruction, a *ghost atom*. In other words, the reconstruction procedure described and used above is not fully reliable, and a re-examination is necessary. This is described in the next section.

3. Development of an improved integral kernel

The basic processes forming the superstructure diffraction spots were already illustrated in figure 1. The complex amplitude in the direction of the detected wave vector $\vec{k}$ of the part of the reference wave due to direct back-scattering from the adatom is denoted by $R_1(\vec{k})$, that (whose scattering paths are denoted by dashed lines in the same figure) from scattering by substrate atoms prior to its scattering by the adatom is defined as $R_2(\vec{k})$ and $O(\vec{k},\vec{r})$ is the object wave due to single scattering of the total reference wave by a substrate atom at position $\vec{r}$ relative to the adsorbate. Of course, all these quantities depend also on the wave vector $\vec{k}_0$ of the incident beam, but for the sake of clarity, we omit this dependence for the moment.

The combined reference wave may be written as

$$R(\vec{k}) = R_1(\vec{k}) + R_2(\vec{k}). \tag{3}$$

where

$$R_2(\vec{k}) = \int \mathrm{d}\vec{r}\ \rho(\vec{k},\vec{r})n(\vec{r}). \tag{4}$$

$\rho(\vec{k},\vec{r})$ is the contribution to R_2 from scattering by a substrate atom at an arbitrary position $\vec{r}$ (neglecting multiple scattering within the substrate) and $n(\vec{r})$ is defined as the distribution of atoms within the substrate (the quantity to be determined) [36–38].

The intensity formed by the interference of the reference and object waves is

$$I(\vec{k}) = \left| R(\vec{k}) + \int \mathrm{d}\vec{r}\ O(\vec{k},\vec{r})n(\vec{r}) \right|^2. \tag{5}$$

Subtracting from the intensity I the term in (5) depending solely on the reference wave R, we may define an 'interference function', $H(\vec{k})$, by

$$H(\vec{k}) \equiv I(\vec{k}) - \left|R(\vec{k})\right|^2 = \int \mathrm{d}\vec{r}\ M(\vec{k},\vec{r})n(\vec{r}) \tag{6}$$

with

$$M(\vec{k},\vec{r}) = \left[R^*(\vec{k})O(\vec{k},\vec{r}) + \text{c.c.}\right] + O^*(\vec{k},\vec{r}) \int \mathrm{d}\vec{r'}\ n(\vec{r'})O(\vec{k},\vec{r'}) \tag{7}$$

where the term within the square brackets represents an 'elementary hologram' [36] and the last term the one involving products of elementary object waves that is usually neglected in holography. (The symbol c.c. denotes the complex conjugate of the term preceding it.)

Even if the quantity R on the LHS is replaced by the so-called 'direct' reference wave R_1, equation (6) is a non-linear equation for the unknown atom distribution $n(\vec{r})$. Iterative procedures for solving equations of such a form have been developed for photoelectron holography [37, 38] and protein crystallography [39, 40]. We will explore the application of similar algorithms in future work (complicated by the fact that the quantity $|R|^2$ on the LHS of (6) is itself a non-linear function of n through R_2). Here, we make two approximations: (a) we replace $R(\vec{k})$ on the LHS of (6) by the directly calculable quantity $R_1(\vec{k})$ (so making $H(\vec{k}) = I(\vec{k}) - |R_1(\vec{k})|^2$ a known signal) and (b) we make the usual holographic approximation of neglecting the quadratic object wave terms in (7). With these approximations, equation (6) reduces to a linear Fredholm integral equation of the first kind [41], if the quantity $M(\vec{k},\vec{r})$ is assumed known. Formally, it may be solved by multiplication with an auxiliary function $Q(\vec{k},\vec{r})$ and subsequent integration over the whole of k-space, i.e.

$$\int \mathrm{d}\vec{k}\ Q(\vec{k},\vec{r})H(\vec{k}) = \int \mathrm{d}\vec{r'}\ n(\vec{r'}) \int \mathrm{d}\vec{k}\ Q(\vec{k},\vec{r})M(\vec{k},\vec{r'}).$$

This leads to

$$n(\vec{r}) = \int \mathrm{d}\vec{k}\ Q(\vec{k},\vec{r})H(\vec{k}) \tag{8}$$

provided that $Q(\vec{k},\vec{r})$ satisfies the condition

$$\int \mathrm{d}\vec{k}\ Q(\vec{k},\vec{r})M(\vec{k},\vec{r}') = \delta(\vec{r}-\vec{r}'). \tag{9}$$

With the above approximations, the function $M(\vec{k},\vec{r})$ may be written as follows:

$$M(\vec{k},\vec{r}) = \left[R_1^*(\vec{k}) + \int \mathrm{d}\vec{r}'\ n(\vec{r}')\rho^*(\vec{k},\vec{r}')\right] O(\vec{k},\vec{r}) + \text{c.c.} \tag{10}$$

The presence of the function n in (10) violates the Fredholm requirement that $M(\vec{k},\vec{r})$ be completely known. Nevertheless, as we see below, in a full application of this algorithm we take n in M to be that found from an earlier iteration in practice. The same holds for the interference function $H(\vec{k})$ itself, as it results by subtraction of $|R(\vec{k})|^2$ from the measured intensity $I(\vec{k})$. Effectively, this *does* make (6) the said linear Fredholm equation at each iteration.

In order to find a practical auxiliary function $Q(\vec{k},\vec{r})$, we take

$$R_1(\vec{k}) = f_b(\vec{k}_0,\vec{k}) \tag{11}$$

$$\rho(\vec{k},\vec{r}) = f_s(\vec{k}_0,-\vec{r})\,f_b(-\vec{r},\vec{k})\frac{\mathrm{e}^{\mathrm{i}(kr+\vec{k}_0\cdot\vec{r})}}{r} \tag{12}$$

and

$$O(\vec{k},\vec{r}) = f_b(\vec{k}_0,\vec{r})\,f_s(\vec{r},\vec{k})\frac{\mathrm{e}^{\mathrm{i}(kr-\vec{k}\cdot\vec{r})}}{r} \tag{13}$$

where the expressions for ρ and O account only for single scattering by the substrate. In the above, the atomic scattering factors $f_{b,s}$ are those of the (adatom) beam splitter (b) or substrate atoms (s). The scattering factors are functions of the electron energy and the scattering angle through the well known expression

$$f(\vec{k},\vec{k}') = \frac{1}{k}\sum_l (2l+1)\mathrm{e}^{\mathrm{i}\delta_l(k)}\sin\delta_l(k)\,P_l(\hat{\vec{k}}\cdot\hat{\vec{k}}')$$

where $\delta_l(k)$ and $\hat{\vec{k}}\cdot\hat{\vec{k}}'$ denote the scattering phase shifts and the cosine of the scattering angle, respectively.

The stationary-phase argument [3, 42, 43] suggests that the auxiliary function may be approximated by

$$Q(\vec{k},\vec{r}) = \left[R^*(\vec{k})O(\vec{k},\vec{r})\right]^{-1}.$$

Substituting from (3), (4), (11), (12) and (13), this can be written explicitly as

$$Q(\vec{k},\vec{r}) = \frac{r\mathrm{e}^{-\mathrm{i}(kr-\vec{k}\cdot\vec{r})}}{\left[f_b^*(\vec{k}_0,\vec{k}) + R_2^*(\vec{k})\right] f_b(\vec{k}_0,\vec{r})\,f_s(\vec{r},\vec{k})} \tag{14}$$

with

$$R_2(\vec{k}) = \int \mathrm{d}\vec{r}'\ n(\vec{r}')\,f_s(\vec{k}_0,-\vec{r}')\,f_b(-\vec{r}',\vec{k})\frac{\mathrm{e}^{\mathrm{i}(kr'+\vec{k}_0\cdot\vec{r}')}}{r'}. \tag{15}$$

This suggests a reconstruction algorithm:

$$n(\vec{r}) = \int \mathrm{d}\vec{k}\ K(\vec{k},\vec{r})\mathrm{e}^{-\mathrm{i}(kr-\vec{k}\cdot\vec{r})}H(\vec{k})$$

with a kernel

$$K(\vec{k},\vec{r}) = \frac{r}{\left[f_b(\vec{k}_0,\vec{r}) + C(\vec{k})\right] f_b^*(\vec{k}_0,\vec{k})\, f_s(\vec{r},\vec{k})} \tag{16}$$

where

$$C(\vec{k}) = R_2^*(\vec{k})\, f_b(\vec{k}_0,\vec{r})/f_b^*(\vec{k}_0,\vec{k}). \tag{17}$$

Since the expression (17) for $C(\vec{k})$ contains the quantity $R_2(\vec{k})$, which involves an integral over the very distribution ($n(\vec{r})$) sought, it can only strictly be evaluated by some sort of iterative scheme in which a first estimate of $n(\vec{r})$ is substituted back into (15) and the procedure iterated to self-consistency.

This was avoided in our earlier approximation to the kernel (2) by replacing $C(\vec{k})$ by an adjustable constant parameter. That kernel also neglected the (relatively small) angular variations of the *back*-scattering factors $f_b^*(\vec{k}_0,\vec{k})$ and $f_s(\vec{r},\vec{k})$ in (17) by treating them as constants. The approximation to the kernel (16) employed in the work described in the next section retains the explicit forms of these scattering factors, but avoids the integral in (15) by neglecting altogether the term $C(\vec{k})$. That is, our present approximation to K is

$$K_2(\vec{k},\vec{r}) = \frac{r}{f_b(\vec{k}_0,\vec{r})\, f_b^*(\vec{k}_0,\vec{k})\, f_s(\vec{r},\vec{k})}. \tag{18}$$

Ultimately, of course, the correct procedure would be to develop an iterative algorithm (which may be an order of magnitude more time consuming) to properly evaluate K (and H) from (16), (17), (4) and (12). The expressions (2) and (18) are both approximations to the full kernel which avoid the self-consistency iterations. The main purpose of the present paper is to point out that the problem we have encountered with the approximation K_1 in the occasional generation of a ghost atom on the high-symmetry axis directly below the adatom beam splitter may be overcome with the use of the alternative approximation K_2.

4. Elimination of the ghost atom

In this section we test our new kernel (18) above, and demonstrate that it enables the reconstruction of reliable real-space images without the appearance of a ghost atom. As a first step, reconstructions were performed using calculated intensities of the 6H-SiC(000$\bar{1}$)-$(2\times 2)_\mathrm{C}$ best-fit structural model. In order to avoid running into possible difficulties arising from different domains and surface terminations, we applied the algorithm to each of the terminations S_1, S_2, S_3 separately. The intensities were calculated for single S_i domains (which give rise to a threefold-symmetric diffraction patterns), and also mixed with those from the rotated S_i^* domain (to give a sixfold-symmetric patterns). The data from I/E curves of a total of 13 beams (for a single domain) were taken as input to the reconstruction algorithm.

The resulting real-space images of the S_1 and S_2 surface terminations are displayed in figure 6 and figure 7, respectively, where the left- and right-hand panels correspond to reconstructions from the corresponding single-domain threefold-symmetric and the mixed-domain sixfold-symmetric data, respectively. (The results for the S_3 termination are not shown, as the local adatom geometry is not much different from that of the S_2 termination.) All images span a cylinder of radius 2.0 Å and depth 7.0 Å below the beam splitter. The scattering factors of both the adatom and substrate atoms were taken to be those of Si.

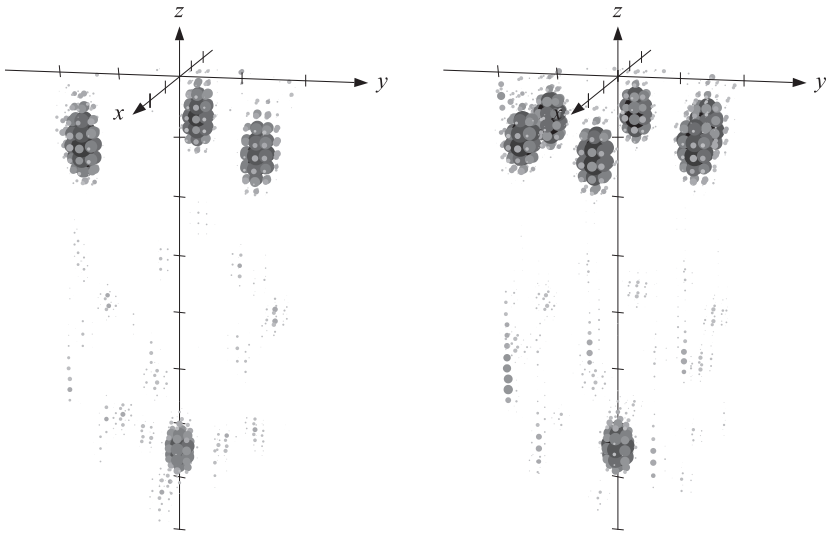

Figure 6. Atomic images reconstructed from calculated intensities of the S_1 surface termination of the 6H-SiC$(000\bar{1})$-$(2 \times 2)_C$ best-fit structure model. The left (right) panel correspond to threefold-symmetric (sixfold-symmetric) data. The electron energy range of the data used is 129–351 eV; the noise level below which image signals are cut off is 20% of the maximum.

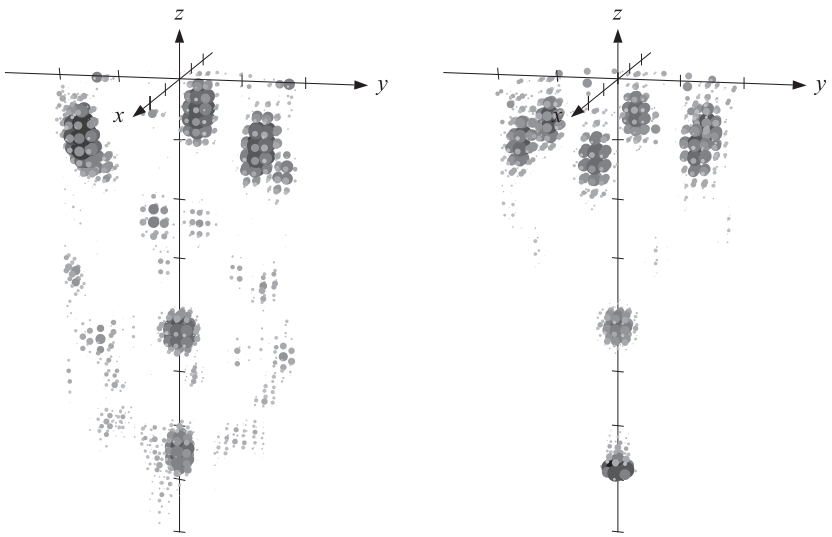

Figure 7. As figure 6, but for the S_2 surface termination.

Clearly, the images allow for an unambiguous identification of the H_3 hollow site from either the single-domain threefold data or the mixed-domain sixfold data. The ghost atom from the use of the previous integral kernel is totally absent, with no remaining image artifact, and no appearance of any new ghost atom. The different local adatom geometries for the S_1 and S_2 terminations are clearly retrieved, with the use of an integral kernel devoid of a free parameter like the quantity C of the previous kernel (2). Once again, no carbon atoms show up in the images due to their weak scattering compared to silicon. This is independent of whether

Si or C scattering factors are used for those of the beam splitter or substrate atoms.

The positions of all atomic images are accurate to within 0.3 Å, as judged from the result of the conventional analysis [23]. This is remarkable in view of the strong buckling (of up to 0.22 Å), within the topmost two SiC bilayers, since deviations from bulk-like positions in the substrate contribute intensity to fractional-order spots or, viewing it another way, act as additional beam splitters [21]. Apparently, in our case the buckling of substrate atoms does not seriously affect the recovered image, presumably because its contributions to the LEED intensities do not match the phase factors in the reconstruction integral (16) giving rise to the above-mentioned stationary-phase conditions.

We also applied the new integral kernel to experimental data. Compared to the calculated data, the experimental data set is considerably smaller in size in respect of the number of fractional-order spots as well as the total energy range. Nevertheless, the same clear atomic image results, as demonstrated in figure 8. Also, the atomic positions are retrieved with the same accuracy, i.e., less than about 0.3 Å from the true positions.

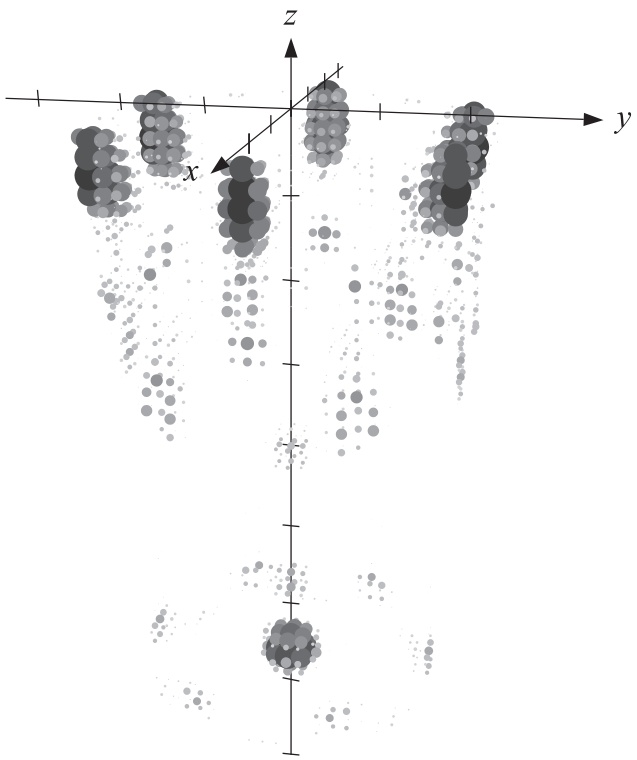

Figure 8. A real-space image reconstructed from experimental data for the 6H-SiC(000$\bar{1}$)-$(2 \times 2)_C$ surface phase. The electron energy range of the data used is 135–349 eV; the noise level is 15%.

5. Discussion and conclusions

The method of directly recovering from a set of LEED I/E data a 3D image of the local atom arrangements in the vicinity of an adatom on a surface by means of a holographic algorithm has had spectacular success recently in helping to solve the structure of SiC(111)-(3×3) that may have offered great resistance to conventional LEED analysis due to the complexity of its

surface reconstruction [17, 18]. When applied to the $(2 \times 2)_C$ phase of 6H-SiC(000$\bar{1}$), however, which also contains a single adatom per surface unit cell, as revealed by scanning tunnelling microscopy, the same holographic algorithm reconstructs a false (or 'ghost') atom image on the high-symmetry axis perpendicular to the surface and directly below the adatom (although the positions of other nearby atoms are correctly reproduced).

In an attempt to ascertain the causation of this ghost atom, we re-examined the current theory of holographic LEED. Our conclusion is that although the general framework of the 'compensated object and reference wave reconstruction by an energy-dependent Cartesian transform' (or CORRECT) theory remains valid, an alternative approximation to the kernel included in the reconstruction integral appears to improve the computed images, with an elimination of the ghost image, and with nearby atom positions determined to a high degree of accuracy.

We also suggest a practical method of calculating an even more accurate kernel, based on an iterative procedure. The scattering of an incident electron by the substrate *prior* to its first encounter with the adatom is correctly treated to the order of single scattering by the substrate atoms. The main consequence is the discovery of a practical method of computing the term denoted by the symbol C in the previous version of the kernel, where that quantity was treated essentially as a constant adjustable parameter. The method that we propose for the calculation of this quantity depends on a prior calculation of an atom distribution function n by the approximate algorithm of this paper (where R_2 and so C are set to zero). The distribution n from that first iteration is then used to estimate the quantity R_2 (and so calculate C and modify H), which quantifies the effect of the prior substrate scattering for the next iteration of the algorithm. It is proposed that the iterations be repeated to self-consistency of the distribution n.

Acknowledgments

This work was supported by Deutsche Forschungsgemeinschaft (DFG) through Sonderforschungsbereich 292, and by the US National Science Foundation (NSF), through grant number DMR-9815092.

References

[1] Saldin D K and De Andres P L 1990 *Phys. Rev. Lett.* **64** 1270
[2] Pendry J B and Saldin D K 1984 *Surf. Sci.* **145** 33
[3] Barton J J 1988 *Phys. Rev. Lett.* **61** 1356
[4] Saldin D K 1997 *Surf. Rev. Lett.* **4** 441
[5] Saldin D K and Chen X 1995 *Phys. Rev.* B **52** 2941
[6] Szöke A 1986 *Short Wavelength Coherent Radiation: Generation and Applications (AIP Conf. Proc. No 147)* ed D J Atwood and J Boker (New York: American Institute of Physics)
[7] Barton J J and Terminello L J 1991 *The Structure of Surfaces III* ed S Y Tong *et al* (Berlin: Springer)
[8] Tong S Y, Hua Li and Huang H 1991 *Phys. Rev. Lett.* **67** 3102
[9] Barton J J 1991 *Phys. Rev. Lett.* **67** 3106
[10] Wei C M and Tong S Y 1992 *Surf. Sci.* **274** L577
[11] Wei C M, Tong S Y, Wedler H, Mendez M A and Heinz K 1994 *Phys. Rev. Lett.* **72** 2434
[12] Heinz K and Wedler H 1994 *Surf. Rev. Lett.* **1** 319
[13] Saldin D K, Chen X, Vamvakas J A, Ott M, Wedler H, Reuter K, Heinz K and De Andres P L 1997 *Surf. Rev. Lett.* **4** 991
[14] Saldin D K, Reuter K, De Andres P L, Wedler H, Chen X, Pendry J B and Heinz K 1996 *Phys. Rev.* B **54** 8172
[15] Mendez M A, Glück C and Heinz K 1992 *J. Phys.: Condens. Matter* **4** 999
[16] Heinz K, Döll R, Wagner M, Löffler U and Mendez M A 1993 *Appl. Surf. Sci.* **70/71** 367
[17] Reuter K, Bernhardt J, Wedler H, Schardt J, Starke U and Heinz K 1997 *Phys. Rev. Lett.* **79** 4818

[18] Starke U, Schardt J, Bernhardt J, Franke M, Reuter K, Wedler H, Heinz K, Furthmüller J, Käckel P and Bechstedt F 1998 *Phys. Rev. Lett.* **80** 758
[19] Heinz K, Starke U and Bothe F 1991 *Surf. Sci.* **243** L70
[20] Heinz K, Starke U, Van Hove M A and Somorjai G A 1992 *Surf. Sci.* **261** 57
[21] Reuter K, Vamvakas J A, Saldin D K, Blum V, Ott M, Wedler H, Döll R and Heinz K 1998 *Phys. Rev.* B **58** 4102
[22] Heinz K, Starke U and Bernhardt J 2000 *Prog. Surf. Sci.* **64** 1631
[23] Seubert A, Bernhardt J, Nerding M, Starke U and Heinz K 2000 *Surf. Sci.* **454–456** 45
[24] Harris G L (ed) 1995 *Properties of Silicon Carbide (EMIS Datareviews Series No 13)* (London: IEE)
[25] Bernhardt J, Nerding M, Starke U and Heinz K 1999 *Mater. Sci. Eng.* B **61+62** 207
[26] Heinz K 1988 *Prog. Surf. Sci.* **27** 239
[27] Reuter K, Wedler H, Ott M, Heinz K, Vamvakas J A, Chen X and Saldin D K 1997 *Phys. Rev.* B **55** 5344
[28] Pendry J B 1974 *Low-Energy Electron Diffraction* (London: Academic)
[29] Van Hove M A and Tong S Y 1986 *Surface Crystallography by LEED* (Berlin: Springer)
[30] Rous P J, Pendry J B, Saldin D K, Heinz K, Müller K and Bickel N 1986 *Phys. Rev. Lett.* **57** 2951
[31] Heinz K, Kottcke M, Löffler U and Döll R 1996 *Surf. Sci.* **357+358** 1
[32] Starke U, Schardt J, Bernhardt J, Franke M and Heinz K 1997 *Phys. Rev. Lett.* **82** 2107
[33] Northrup J E and Neugebauer J 1995 *Phys. Rev.* B **52** R17 001
[34] Pollmann J, Krüger P and Sabisch M 1997 *Phys. Status Solidi* b **202** 421
[35] Pendry J B 1980 *J. Phys. C: Solid State Phys.* **13** 937
[36] Szöke A 1993 *Phys. Rev.* B **47** 14 044
[37] Saldin D K, Chen X, Kothari N and Patel M H 1993 *Phys. Rev. Lett.* **70** 1112
[38] Chen X and Saldin D K 1994 *Phys. Rev.* B **50** 17 463
[39] Saldin D K, Shneerson V L and Wild D L 1997 *J. Imaging Sci. Technol.* **41** 482
[40] Szöke A, Szöke H and Somoza J R 1997 *Acta Crystallogr.* A **53** 291
[41] Press W H, Teukolsky S A, Vetterling W T and Flannery B P 1992 *Numerical Recipes in FORTRAN* (Cambridge: Cambridge University Press)
[42] Tonner B P, Han Z L, Harp G R and Saldin D K 1991 *Phys. Rev.* B **43** 14 423
[43] Saldin D K, Harp G R and Tonner B P 1992 *Phys. Rev.* B **45** 9629